2015

Comparison between single band and concurrent multi-band linear power amplifiers

Zhen Zhang
Iowa State University

Comparison between single band and concurrent multi-band linear power amplifiers

by

Zhen Zhang

A thesis submitted to the graduate faculty

in partial fulfillment of the requirements for the degree of

MASTER OF SCIENCE

Major: Electrical Engineering

Program of Study Committee:
Nathan M. Neihart, Major Professor
Degang Chen
Santosh Pandey

Iowa State University

Ames, Iowa

2015

TABLE OF CONTENTS

LIST OF FIGURES

LIST OF TABLES

NOMENCLATURE

LTE	Long–Term Evolution
PA	Power Amplifier
RF	Radio Frequency
MOSFETs	Metal-Oxide-Semiconductor Field-Effect Transistors
PAE	Power-Added Efficiency
AM	Amplitude Modulation
IMs	Intermodulations
IMD	Intermodulation Distortion
IIP3	Third-Order Intercept Point
PAR	Peak-To-Average Ratio

ACKNOWLEDGMENTS

I would like to express the appreciation to my committee chair, Dr. Nathan M. Neihart, for his excellent guidance, patience, and providing me with a very good chance for doing research. I would also thank my committee members, Dr. Degang Chen, and Dr. Santosh Pandey, for helping me develop my background in integrated circuit and semiconductor devices.

In addition, I would also like to thank my friends, lab mates, the department faculty and staff for making my time at Iowa State University a wonderful experience.

Finally, thanks to my parents for their encouragement. They were always supporting me and encouraging me with their best wishes.

ABSTRACT

Currently the multiple wireless data transmission technologies have been commercially implemented, such as long-term evolution (LTE), Wi-Fi, and Bluetooth. There is a keen requirement to combine the power amplifiers for those technologies into a single one which can amplifies concurrent multi-band signals. On the physically layer, there are two popular architectures, namely parallel single-band power amplifiers and concurrent multi-band power amplifiers.

In this thesis, quantitative comparison between parallel single-band power amplifiers and concurrent multi-band power amplifiers has been presented theoretically in the aspects of area, drain efficiency and linearity. Methods of calculating drain efficiency is derived for concurrent multi-band PAs for different frequency ratios. Linearity issues of concurrent multi-band power amplifiers have been addressed based on the concepts of gain compression and intermodulation distortion.

Final, area consumption has been compared for both architectures with current technologies. Results of the drain efficiency map versus 2-D frequency ratio are plotted in figures for class A, B and C. Linearity degradation of concurrent multi-band has been derived mathematically.

CHAPTER 1

INTRODUCTION

1.1 Recent Developments of Wireless Technologies

Modern wireless communication industry has become a critical business and necessary part of daily life in most countries around the world [1]. Varieties of different wireless data technologies are applied in mobile devices such as long-term evolution (LTE), Wi-Fi, and Bluetooth. Those technologies are allocated in different spectrums as Fig. 1 shows.

The conventional design contains one power amplifier for each technology which occupies large area. Moreover the more number of components are translated into the higher cost. Therefore, there is a keen motivation to develop multi-band power amplifier (PA) in order to reduce cost and physical size.

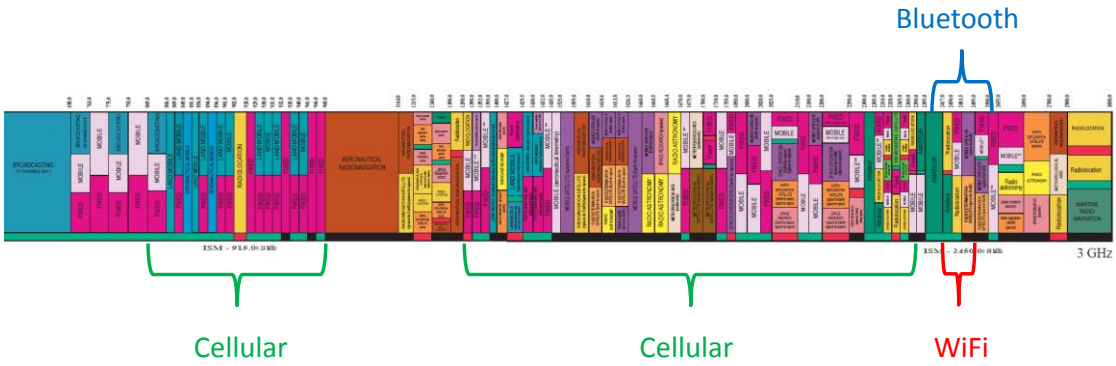

Figure 1. *Frequency allocations of wireless data technologies. [2]*

1.2 Motivation

Multi-band power amplifiers can support signals of multiple band frequencies simultaneously, therefore all wireless functions can work at the same time. Many PA architectures and techniques are developed [3]. Among them, there are two popular architectures, namely parallel single-band PAs and concurrent multi-band PAs.

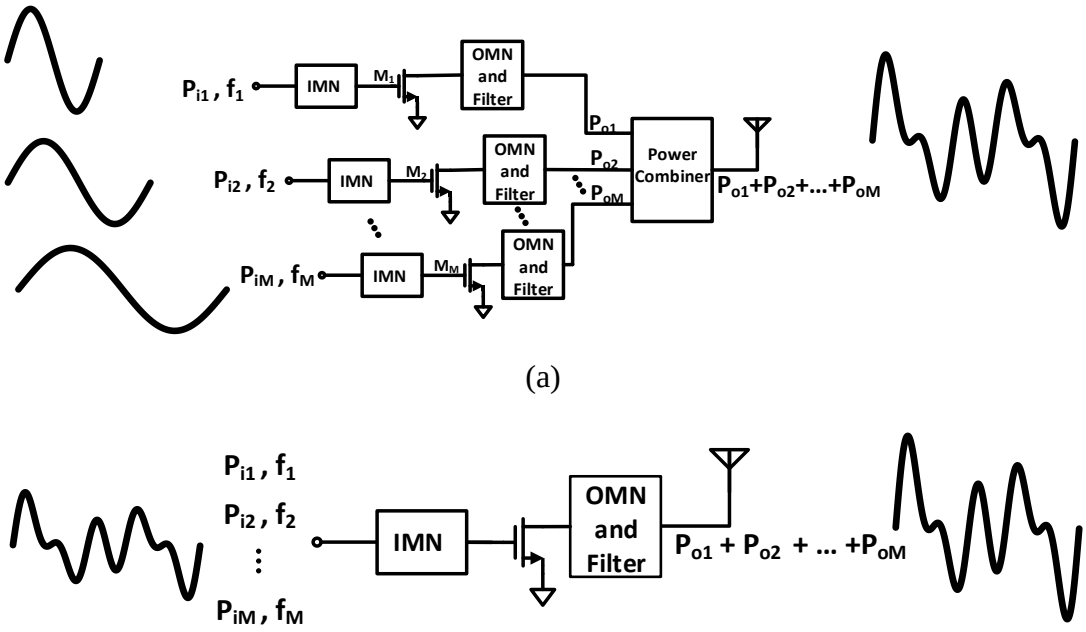

Figure 2. *Candidates of power amplifier for CA in LTE-advanced systems: (a) multiple branch PA and (b) concurrent multi-band PA*

In the architecture shown in Fig. 2(a), the PA has multiple branches of conventional single-band PAs with a multi-band power combiner [4]. Each branch only amplifies signal of single-band, therefore the theory of each branch are fully developed. Then signals of all frequency bands are combined at power combiner. Therefore, the performance of the power

combiner is critical to the whole PA. This architecture is referred as parallel single-band PA which can support concurrent multi-band operation.

Instead of using multiple transistors, the other architecture shown in Fig. 2(b) uses a single transistor with both input and output multi-band matching networks [5-7] which are usually based on prototype-filter transformation techniques. This architecture is known as concurrent multi-band PAs. The concurrent multi-band PAs has the capability of amplifying multi-frequencies signals simultaneously. However, one of the drawback of the concurrent multi-band PA is that the drain efficiency will drop when the number of bands increases. One example of the efficiency drop for concurrent dual-band is shown in [8].

At this point, the theory of conventional single-band power amplifier cannot provide an accurate prediction of the performance of concurrent multi-band PAs. And current work [8] has two limitations. The first one is that it only shows the analysis of concurrent dual-band, which is not generalized to multi-bands. The second one is that it only concerns the effect of different amplitudes. However, different frequency ratio also have effects on drain efficiency and linearity performance of concurrent multi-band PAs.

Therefore, this thesis will focus on providing quantitative methods for a comparison in efficiency and linearity performances between the two architectures which are parallel single-band PA and concurrent multi-band PA in class-A, class-B, and class-C. The comparison includes three aspects, namely area consumption, drain efficiency and linearity.

1.3 Overview Of The Work And Its Contribution

Chapter 2 reviews the conventional single-band linear PAs in all three classes. Chapter 3 focuses on the derivation of the performances of concurrent multi-band PAs. In Chapter 4, the simulation results are presented and comparison analysis is given. Chapter 5 concludes by summarizing the advantages and disadvantages of both architectures. The contribution of this thesis is to give a guidance for the PA designers that which architecture will theoretically have better performance and their limitations.

CHAPTER 2

REVIEW OF CONVENTIONAL SINGLE-BAND LINEAR POWER AMPLIFIER

In order to explore the properties of dual-band or multi-band PAs, it is necessary to reviews the classification of single-band power amplifiers. Then it is followed with critical properties of single-band linear PAs, namely are the drain efficiency and linearity. The reason why the derivations are represented here is that the theories of multi-band PAs are based on conventional single-band power amplifiers.

2.1 Architecture of Single-Band Linear PAs

The schematic of classical power amplifier is shown in Fig. 3 where IMN, OMN are the input matching network and output matching network, and DCB is the DC block capacitor. All transistors in the thesis are metal-oxide-semiconductor field-effect transistors (MOSFETs) [9]. Two voltage bias circuits are placed at gate and drain of the transistor which source are tied to ground. The radio frequency (RF) signals are isolated by RF chock inductors and bypassed by capacitors. Here the input matching network and output matching network are represented as blocks because there are many options to implement narrow single-band matching networks, such as L-, T- and Pi-match.

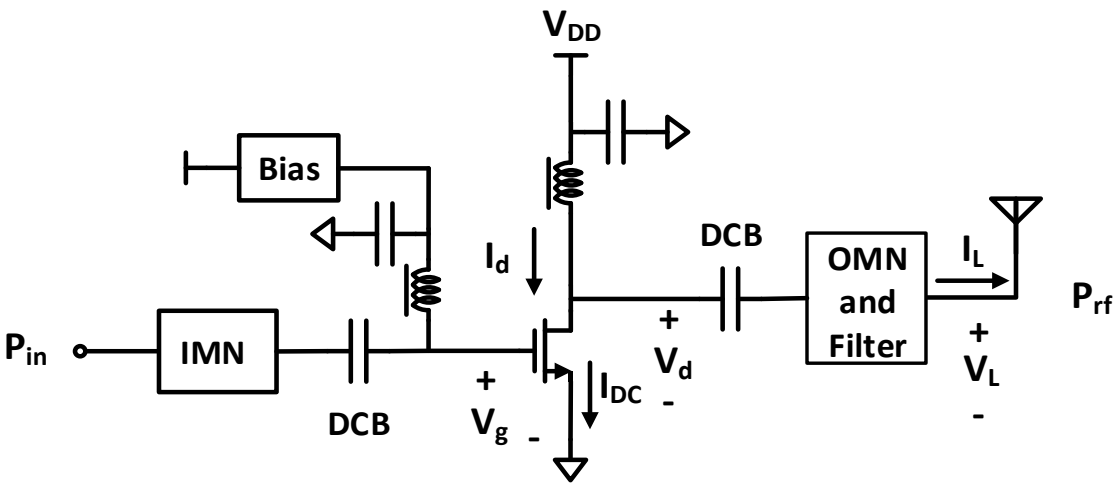

Figure 3. *Schematic of RF power amplifier with blocks*

2.2 Classification of PA

Power amplifiers in general can be classified into two main categories, namely linear PAs and switch mode PAs. For a linear RF PAs, the transistors will work in saturation region, where drain current I_d is nearly proportional to the magnitude of gate voltage V_g. Generally, the linear power amplifiers have higher linearity but lower efficiency. However, the transistors of switch mode power amplifiers must remain ohmic region when it is on and in the cutoff region when it is off. The switching functioning generates less time of a period that both current voltage have high instant values. Therefore the efficiency of switch mode PAs normally are higher than linear PAs. However, switching RF power amplifier always have worse linearity than linear amplifier. One of the reasons is that the switching transistor ignores the amplitudes verification of input signal. Since many of the modern wireless communication technologies requires amplitude modulation, in this thesis, only linear RF power amplifiers are discussed.

The classification of linear RF PAs is represented by the conduction angle 2θ which reveals the percentage of conducting time of the transistor to an entire signal period. Class-A

has 360° conduction angle which indicates the transistor is always on. When transistor is on, the gate voltage V_g is higher than threshold voltage V_t. For an ideal transistor, the threshold voltage is zero. The conduction angle of class-B 2θ is 180° which means the transistor will conducting for half of the cycle. The conduction angle of class-AB is between class-A and class-B that $180° < 2\theta < 360°$. While for class-C the conduction angle 2θ is less than 180°.

The Fig. 6 shows the bias points for all four linear classes as green dots. Blue curves represents the drain current wave forms, which solid one is class A and dashed curve is class B. Red curve is drain voltage waveform.

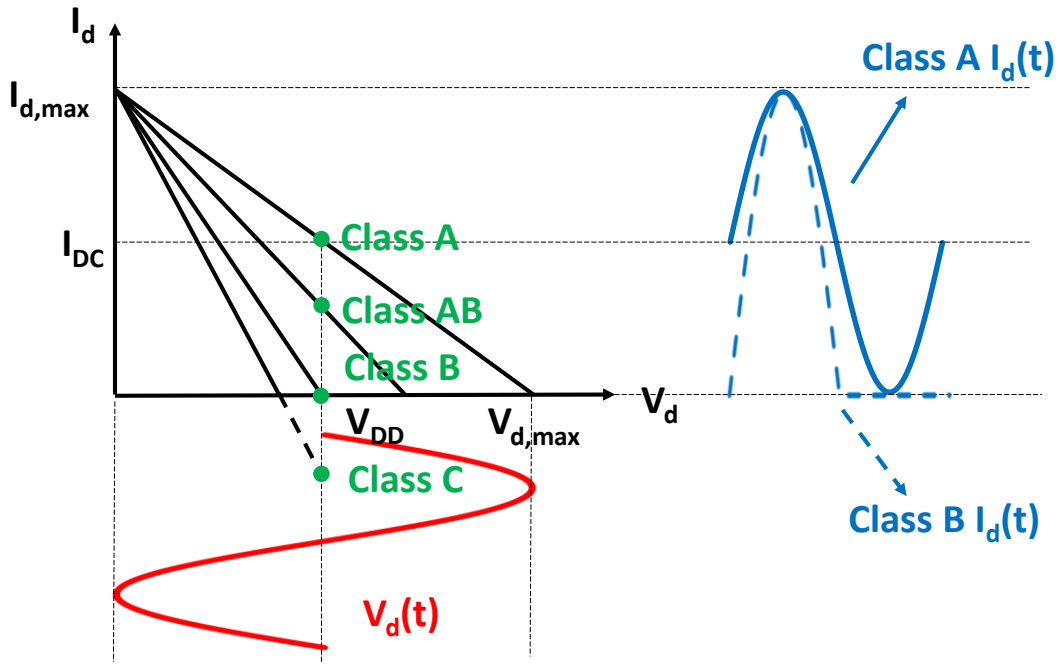

Figure 4. *Bias points of Class-A, class-B, class-AB, and class-C and operation modes of Class-A, and class-B*

2.3 Drain Efficiency of Single-band

One of the most important performances for a PA is its drain efficiency, because PA is the most power hungered device among the transmitter. Efficiency measures how much DC power is turned into RF power by the power amplifier. Beside power consumption, the low efficiency will also cause thermal issue and of the transmitter. Generally, two main methods are used to define efficiency of MOSFET PAs with wide acceptance. The first one is drain efficiency which has the expression as:

$$\eta_D = \frac{P_{RF}}{P_{DC}}, \tag{1}$$

where P_{RF} is the power of output RF signal, and P_{DC} is DC power consumption from power supply. Drain efficiency can represent the efficiency characters of PAs sufficiently when the PA has a high gain. The more accurate method is to calculate power-added efficiency (PAE) which has the expression:

$$\eta_{PAE} = \frac{P_{RF}-P_{in}}{P_{DC}}. \tag{2}$$

where P_{in} is the input power of RF signal. However, PAE is normally used in the specification of measurement or simulation which requires a specific model of the transistor.

Since the efficiency derivation in this thesis is a general solution, rather than for a specific transistor model, the efficiency of PAs will be discussed in only the form of drain efficiency.

2.3.1 Drain Efficiency of Class-A Power Amplifier

For an ideal class-A PA, in order to maintain the transistor conducting all time, the biasing condition is the gate voltage should be always higher than V_t and DC component of drain voltage V_{DD} should maintain the minimum value of drain voltage above zero. The voltage and current waveforms are shown in the Fig. 6. Both load current I_L and V_L are pure sinusoidal signal, because of the DC block capacitors. The expression of drain current and drain voltage waves are:

$$\begin{aligned} I_d(t) &= I_{DC} + I_L \cos \omega t \\ V_d(t) &= V_{DD} - V_L \cos \omega t. \end{aligned} \tag{3}$$

where the I_{DC} and V_{DD} are the DC components of drain current and drain voltage. In order to maintain the high linearity, the amplitudes of load current and voltage should be lower than or equal to the value of DC components:

$$\begin{aligned} I_{DC} &\geq I_L \\ V_{DD} &\geq V_L. \end{aligned} \tag{4}$$

Therefore, the maximum efficiency occurs at the point where the waveforms have $I_L = I_{DC}$ and $V_L = V_{DD}$. Therefore, the maximum theoretical efficiency only happens when both the ac drain current and voltage swing or amplitudes achieve their maximum value without clipping. The expression of max drain efficiency of class-A PA is

$$\eta_d = \frac{P_{RF}}{P_{DC}} = \frac{\frac{I_L V_L}{2}}{I_{DC} V_{DD}} = 50\% \tag{5}$$

2.3.2 Drain Efficiency of Class-B Power Amplifier

One way of improving the efficiency is to reduce the conduction angle, because the overlap between drain voltage and drain current is minimized consequently. When the conduction angle is reduced to 180 degree, it is defined as class-B. Since transistor conduct only half of the signal period, the drain current is clipped as Fig 6 shows. The drain current waveform can be expressed in the form of piecewise function as:

$$I_d = \begin{cases} I_{DC}\sin(\omega t) & 0 < \omega t < \pi \\ 0 & \pi < \omega t < 2\pi \end{cases}. \tag{6}$$

The fundamental component of the drain current is

$$I_{fund} = \frac{1}{\pi}\int_0^{\pi} I_{DC}\sin^2 \omega t \, d(\omega t) = \frac{I_{DC}}{2} = \frac{\pi}{2} I_{avg}. \tag{7}$$

The drain efficiency will reach the maximum value when amplitude of drain voltage equals to the DC voltage supply:

$$V_{fund} = V_{DD}. \tag{8}$$

The theoretical efficiency expression is

$$\eta_d = \frac{P_{RF}}{P_{DC}} = \frac{\frac{I_{fund}V_{DD}}{2}}{\frac{2}{\pi} I_{fund}V_{DD}} = 78.5\% \ . \tag{9}$$

Inevitably, one side-effect is reducing conduction angle causes harmonics. The signal should be filtered before delivering to the antenna and ideally only fundamental components of current and voltage is left.

2.3.3. Drain Efficiency of Class-AB And Class-C Power Amplifier

The theory of class-C PAs is similar with class-B PA. However, the bias point of class-C locates at cutoff region. Transistor maintains off till gate voltage increases higher than its threshold voltage. Therefore, the conduction angle is 2θ which is less than 180 degree. While class-AB has a conduction angle between 180 degree and 360 degree.

The general solution of drain efficiency for both class-AB and class-C has been raised in [10], which the calculation is based on 2θ. The drain efficiency of class-AB is between class-A and class-B. Since class-C has less conduction angle than class-B, it has higher drain efficiency.

In all of these classes, class-A and class-AB PAs are more suitable to mobile units because they have higher gain with less distortion. Class-C PAs are more suitable for base station units which has low gain but high efficiency [11].

2.4 Linearity

Besides the efficiency, another issue caused by non-ideal effects is the linearity of the output signal which becomes substantial to the amplitude modulation (AM). Poor linearity will not only reduce the power generated on the fundamental band but also those power will leak to other bands which are either harmonics or intermodulations (IMs). Therefore, two values are always addressed to analyze the linearity of PAs, namely gain compression and intermodulation distortion (IMD).

To analyze the harmonic distortion ideally, the transistor of power amplifier is driven by a single-tone sinusoidal input voltage:

$$V_g(t) = A\cos(\omega t)\,, \tag{10}$$

where A is the amplitude of the gate-to-source voltage. For simplicity, the power amplifier is assumed as a memoryless time-invariant system. Then the traditional approach is to model the nonlinear transistor by a power series. For simplicity, the approximate power series polynomial is truncated at third-order:

$$\begin{aligned} I_d(t) &= \alpha_0 + \alpha_1 V_g(t) + \alpha_2 V_g^2(t) + \alpha_3 V_g^3(t) \\ &= \alpha_0 + \frac{1}{2}\alpha_2 A^2 + \left(\alpha_1 A + \frac{3}{4}\alpha_3 A^3\right)\cos(\omega t) + \frac{1}{2}\alpha_2 A^2 \alpha_2 \cos(2\omega t) \\ &\quad + \frac{1}{4}\alpha_3 A^3 \alpha_3 \cos(3\omega t). \end{aligned} \tag{11}$$

According to the trigonometric identities, it is apparent that even-order terms of the power series produce DC components and the odd-order terms produces fundamental components of the drain current. Since generally, the coefficient of third-order term α_3 generally has an opposite sign with α_1, gain will decrease along with increasing input amplitude. Therefore 1-

dB compression point is defined the amplitude of the input signal where the power gain of the transfer function drop by 1-dB comparing with linear system, and has an expression:

$$A_{1dB} = \sqrt{\frac{4}{3}\left|\frac{\alpha_1}{\alpha_3}\right| \cdot 0.11}. \tag{12}$$

Another approach to determine amplitude-amplitude (AM-AM) conversion is to analyze intermodulation products. Intermodulation occurs when more than one band signals are applied to the input of non-linear PA. Two frequencies gate voltage will be an example here that input signal has an expression:

$$V_g(t) = A\cos(\omega_1 t) + A\cos(\omega_2 t)\,. \tag{13}$$

Expanding the output signal by power series:

$$\begin{aligned} I_d(t) &= \alpha_0 + \alpha_1 V_g(t) + \alpha_2 V_g^2(t) + \alpha_3 V_g^3(t) \\ &= \alpha_0 + \frac{1}{2}\alpha_2 A^2 + \left(\alpha_1 A + \frac{3}{4}\alpha_3 A^3\right)\cos(\omega_1 t) \\ &\quad + \left(\alpha_1 A + \frac{3}{4}\alpha_3 A^3\right)\cos(\omega_2 t) + \frac{1}{2}\alpha_2 A^2 \alpha_2 \cos(2\omega_1 t) \\ &\quad + \frac{1}{2}\alpha_2 A^2 \alpha_2 \cos(2\omega_2 t) + \frac{1}{4}\alpha_3 A^3 \alpha_3 \cos(3\omega_1 t) \\ &\quad + \frac{1}{4}\alpha_3 A^3 \alpha_3 \cos(3\omega_2 t) + A^2 \alpha_2 \cos(\omega_1 - \omega_2)t \\ &\quad + A^2 \alpha_2 \cos(\omega_1 + \omega_2)t + \frac{3}{4}A^3 \alpha_3 \cos(2\omega_1 - \omega_2)t \\ &\quad + \frac{3}{4}A^3 \alpha_3 \cos(\omega_1 - 2\omega_2)t + \frac{3}{4}A^3 \alpha_3 \cos(2\omega_1 + \omega_2)t \\ &\quad + \frac{3}{4}A^3 \alpha_3 \cos(\omega_1 + 2\omega_2)t. \end{aligned} \tag{14}$$

Therefore, the fundamental component is:

$$A_{fund} = \left(\alpha_1 + \frac{9}{4}\alpha_3 A^2\right) \cdot A. \tag{15}$$

The third-order intercept point (IIP3) is defined as the fundamental amplitude of interception point between the first order $\alpha_1 A$ and the third order $\frac{9}{4}\alpha_3 A^2$, which is shown in Fig. 4. The amplitude of IIP3 has the expression:

$$A_{IIP3} = \sqrt{\frac{4}{3}\left|\frac{\alpha_1}{\alpha_3}\right|}. \tag{16}$$

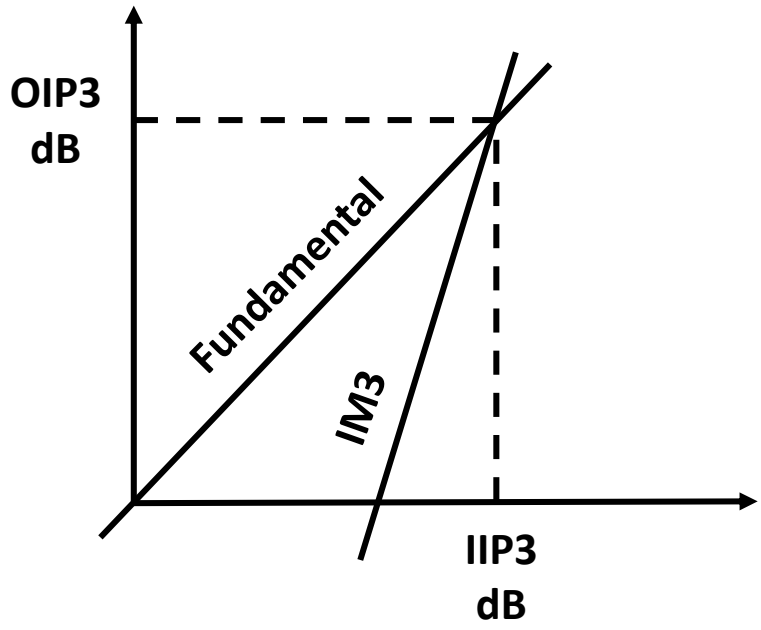

Figure 5. *3rd order interception point*

Other than the effects on fundamental frequency, the IM products also leaks power to sidebands which is shown in Fig 5. Those sidebands tones might block the signal of other bands or cause distortion.

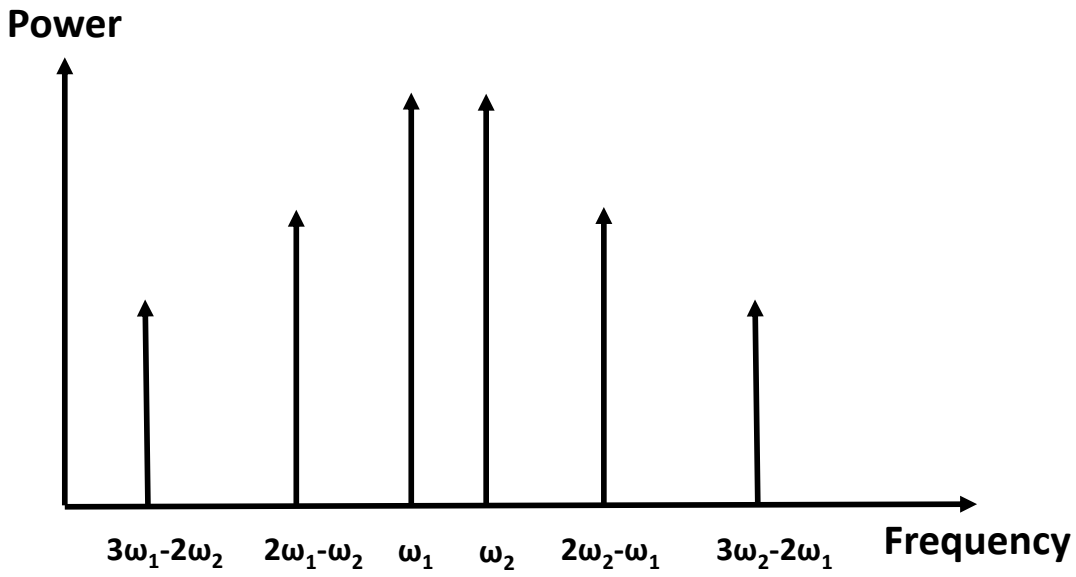

Figure 6. *The spectrum of two-tone IM products*

CHAPTER 3

CONCURRENT MULTI-BAND POWER AMPLIFIER

As mentioned in Chapter 1, two main architectures of concurrent multi-band PAs, namely parallel single-band and concurrent multi-band which are shown in Fig. 7. The idea of which architecture has more benefits in physically implementing such as cost, area is not developed. The other question is which has better performances in drain efficiency or linearity. Since the theory of both architecture are not compete, the following sections will introduce the theoretically quantitative analysis of area, drain efficiency and linearity of concurrent multi-band PAs.

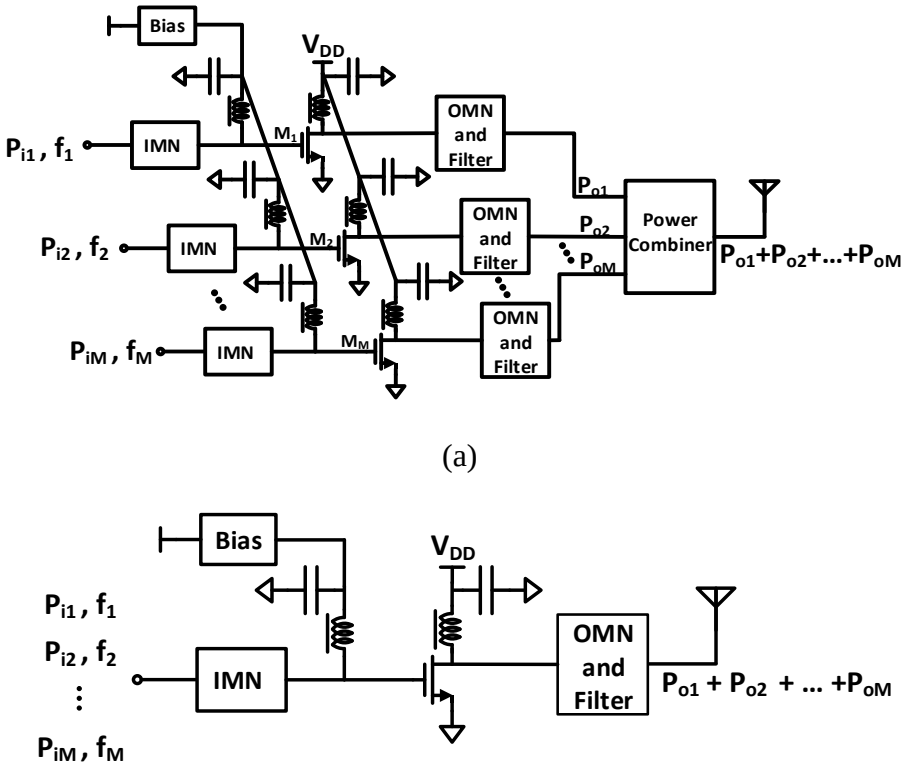

Figure 7*. Schematic showing architectures of (a) parallel single-band power amplifier and (b) concurrent multi-band power amplifier*

3.1 Area Comparison of Two Architectures

As not many designs of the PA are fully integrated for either conventional single-band or concurrent dual-band types and the distributed components has no standard of area, the comparison are all based on lump elements structures. There are 6 types of components in total shown in Fig. 7, namely input/output matching networks, RF chock inductors, bypass capacitors, power combiners and power transistors. In order to analyze the area characteristics of both architecture, it is necessary to know both number of components for each architecture and the size of each component.

The first is to summarize components number for both architectures. When considering the parallel single-band architecture, each branch of the PA will has both input and output matching networks, which at least one matching network is built by two components as L-match. Therefore an M-band architecture will require $2M$ components for each of the matching networks. As both drain and gate of the transistor should be biased properly, the two RF chock inductors and two DC block capacitors are used for every branch, which means $2M$ choke inductors and $2M$ bypass capacitors will be required. Unfortunately, the RF chock inductors and bypass capacitors of different branches are not able to be shared to reduce the number of components. The reason is intuitive that sharing the inductors and capacitors of bias circuits are shorting drains of all branches together and so do gates. Since branches operating under different frequencies, sharing will lead to unacceptable levels of leakage from one band to the next due to the reduced isolation between paths. In addition to the M transistors that will be required, the parallel single-band architecture will also require a power combiner to combine all of the signals together for wireless transmission.

However, there are two limitations of the power combiner which are the large size and high insertion loss. Table 1 lists the performances of power combiners including academic designs and commercial products. It is apparent that even the smallest area in [14] is actually large comparing to normal standard power amplifier. Since the structure of [12-14] are based on Wilkinson power combiners, the insertion losses are all larger than 3 dB. Loss larger than 3 dB means that more than half of the output power will be consumed by the power combiner, which is not acceptable for PA design. The designs of [4,15,16] show low loss since the structures are diplexer or triplexer. In contrast, the diplexer or triplexer will have very high area consumption.

Table 1 Performance of Power Combiner

Reference	Multi-band Frequency(GHz)	Insertion loss (dB)	Area mm^2
[12]	0.9, 1.17 2.43	< 3.4, < 3.4, < 3.4	≈1705
[13]	1, 2.4, 2.07	3.75, 3.66, 3.17	≈9000
[14]	1.02, 2.57, 3.06	3.7, 4.2, 4.0	≈1225
[4]	2.00, 2.05	≈0.73, ≈0.73	≈ 12720
[15]	0.698-0.793/0.824-0.894/1710-2170	< 0.35,<0.4, <0.3	≈ 22590
[16]	0.88-0.96/1.71-2.17	<0.2, <0.2	≈ 34800

The concurrent multi-band architecture saves many components. Comparing to parallel single-band PAs, only one branch exists and amplifies all bands. Only one transistor requires only two RF chock inductors and two bypass capacitors. The power combiner becomes

unnecessary since signals of all bands are mixed at the input port. There is, however, it has the same number of components with parallel single-band architecture. A single-band L-match network can be modified to provide matching at multiple frequencies, which the frequency transformation idea borrowed from filter design is applicable [6]. Intuitively, frequency transformation is to replace low-pass structures to either band-pass or band-stop structures. Since low pass has only one component but both band-pass and band-stop has two components, one more band requires an extra component. Therefore, $2M$ components in total are necessary for M-band input and output matching networks.

The numbers of components for both M-band architectures are summarized in Table 2. That the total number of components of parallel single-band is more than concurrent multi-band architecture. It is seen that the parallel single-band architecture requires M times the number of the choke inductors, bypass capacitors, and transistors compared to the concurrent multi-band architecture.

Table 2. Component Count for Parallel Single-Band And Concurrent Dual-Band Architecture

Component List	Number of Components	
	Parallel Single-band	Concurrent Multi-band
Input L-Match Network	2M	2M
Output L-Match Network	2M	2M
RF Choke Inductor	2M	2
RF Bypass Capacitor	2M	2
Power Combiner	1	0
Power Transistor	M	1
Total	9M+1	4M+5

Secondly, it is necessary to have the size for each component which are listed in Table 3. Since the comparison is under theoretical condition, all components are lump elements consumes because it consumes less area than distributed components. And The RF choke inductors, bypass capacitors, and power transistors are calculated in real technology. The size of power combiner is obtained from [4].

Table 3. Size of Each Component

Component List	Technology	Single Size
Input L-Match Network	0201	0.18 mm^2
Output L-Match Network	0201	0.18 mm^2
RF Choke Inductor	0402	0.5 mm^2
RF Bypass Capacitor	AVX TPME227K016R0025	31.39 mm^2
Power Combiner	[4]	12720 mm^2
Power Transistor	CREE CGH40006P	15.26 mm^2

The Table 4 shows the example of area consumption for both architectures in dual-band, which 20% additional area of components is calculated in for routing. Although the number of components in parallel single-band architecture is much more than concurrent multi-band architecture. However, the area consumption is dominated by the power combiner, since the size of power combiner is hundreds times larger than other components.

Table 4. Size Comparison Example of Dual-band Both Architecture

Component List	Single Size	Parallel Single-band		Concurrent Multi-band	
		Number of components	Area	Number of components	Area
Input L-Match Network	0.18 mm^2	4	0.72 mm^2	4	0.72 mm^2
Output L-Match Network	0.18 mm^2	4	0.72 mm^2	4	0.72 mm^2
RF Choke Inductor	0.5 mm^2	4	2 mm^2	2	2 mm^2
RF Bypass Capacitor	31.39 mm^2	4	62.78 mm^2	2	31.39 mm^2
Power Combiner	12720 mm^2	1	12720 mm^2	0	0
Power Transistor	15.26 mm^2	2	30.52 mm^2	1	15.26 mm^2
Total		19	12816.74 mm^2	13	50.09 mm^2

3.2 Drain Efficiency of Linear Concurrent Multi-Band Linear PA

Since the schematics are the same between the conventional single-band PAs and parallel single band PAs excluding the power combiner, the performance of this architecture is mainly effected by the power combiner. Therefore, this chapter will focus on the behavior of concurrent multi-band architecture.

Calculating the drain efficiency for multi-band linear PAs has the same basic scheme with the single-band, which is the ratio of RF power to DC power consumption. Both strongly and weakly non-linear transistor model shown in Fig. 8 of MOSFET are introduced in this analysis, which the drain current is expressed as [17]:

$$I_d(t) = \begin{cases} 0 & V_g(t) \le 0 \\ 3V_g^2(t) - 2V_g^3(t) & 0 < V_g(t) < 1, \\ 1 & V_g(t) \ge 1 \end{cases} \quad (17)$$

where $V_g(t)$ is the input gate-source voltage for the MOSFET and for M-band it has the expression as:

$$V_g(t) = V_{gDC} + Asin(\omega_1 t) + Asin(\omega_2 t) + \cdots + Asin(\omega_M t), \quad (18)$$

where V_{gDC} is the DC bias voltage and A and ω_M are the amplitude and angular frequency of M-th carrier signal, respectively. Each band has the same amplitude because it is the worst case for efficiency and linearity which is mentioned in [8]. It has an intuitive explanation that the larger the amplitude differences are, the closer the multi-band waveform is to the single-band.

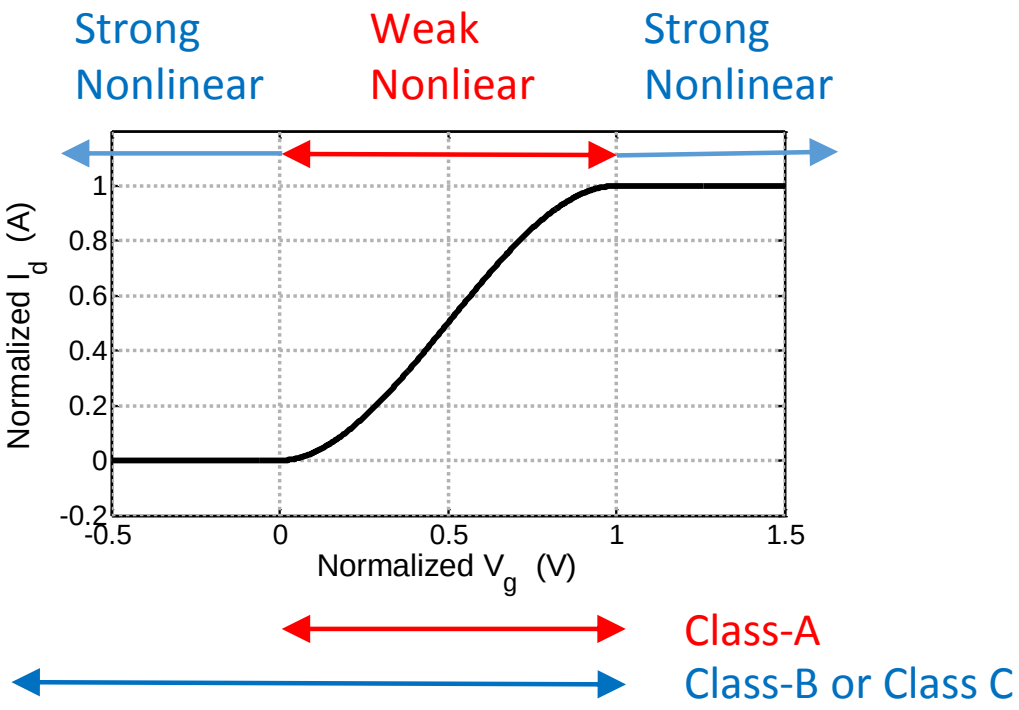

Figure 8. *Transistor transfer function showing both strong and 3rd-order weak nonlinearity*

One thing noteworthy here is that the transfer function (17) requires the gate voltage to be normalized to 1. It is apparent that when $V_g(t)$ value is above 1, the drain current will saturate which is also shown as clipping in the aspect of signal $I_d(t)$. In order to fully utilize the range of V_g but avoid clipping I_d, the next step should be obtaining the maximum value of V_g.

Normally the method of finding the maximum by solving the derivative equals to zero which is $V_g'(t) = 0$. However, $V_g'(t)$ is a transcendental function which means it should be solved by numerical methods, for example the root-finding algorithms. Root-finding algorithms has two main categories which are bracketing methods and open methods. The main difference of the two categories is bracketing methods set the initial upper and lower boundaries.

The first option of bracketing is bisection method. Fig. 9 shows the process of bisection method, where the green dot represents the root. Briefly, it uses the midpoint to replace the upper or lower bound, once the midpoint and bound point value has the same sign. The advantages of this method are robust, simple, and error computable. However, it relies on the initial bracket, and is not able to find multiple roots in one bracket.

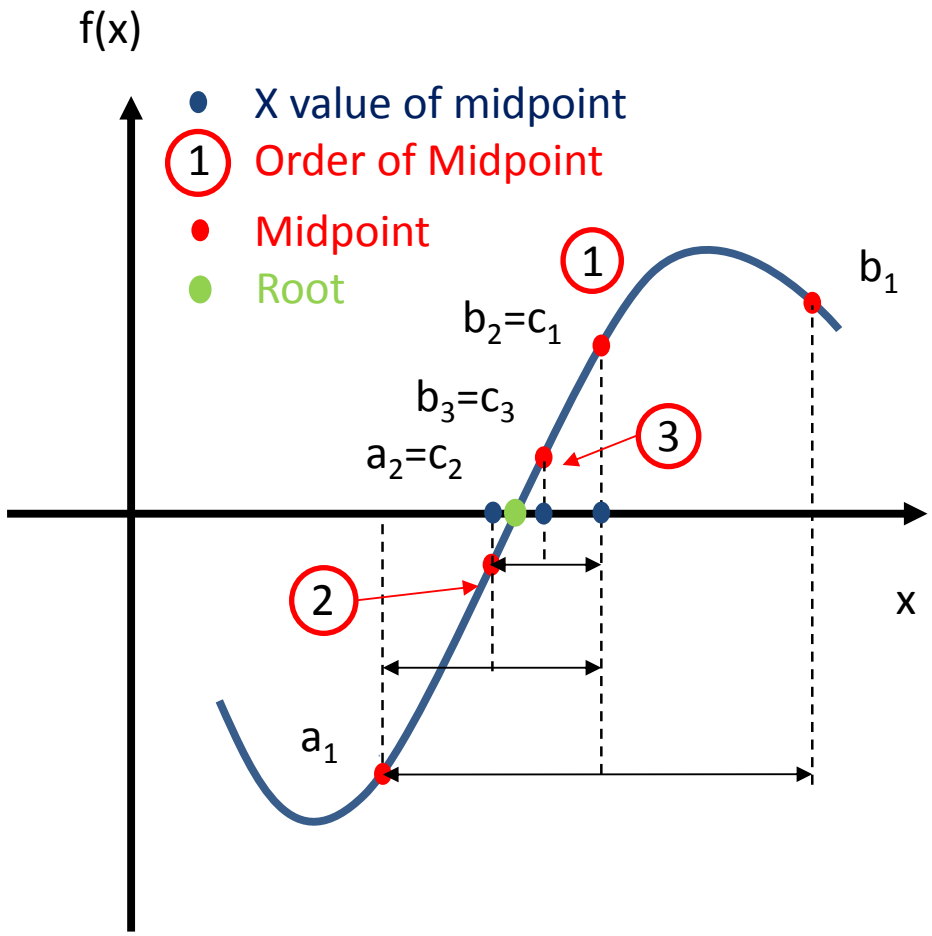

Figure 9. *Process of bisection method*

The second option of bracketing methods is false position method which is shown in Fig. 10. The process of false position method is also very simple. By connecting bracket points, the line will be an interception point. The midpoint of the interception will be the new bracket point till the interception point lies on the root. False position methods is faster than bisection

method. However, it not only requires initial bracket, but also is not as robust as bisection methods.

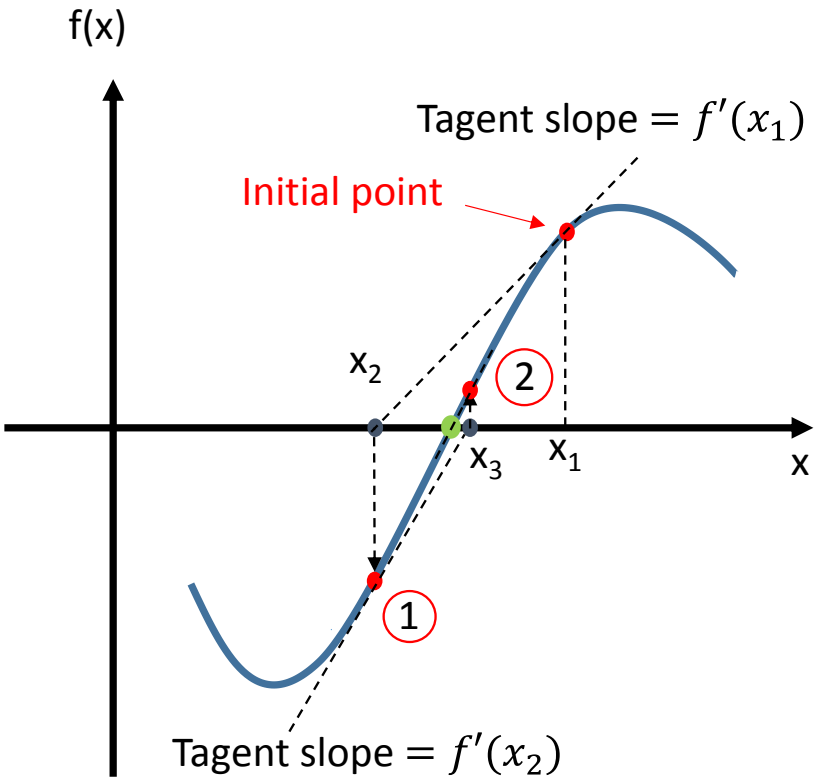

Figure 10. *Process of false position method*

The third one is Newton's method which is shown in Fig. 11. It is one of the open methods. This method use interception point of the tangent line and x-axis to find midpoint. Therefore the convergence to root is fast. However, the convergence speed is determined by the initial point and the slope of the tangent line.

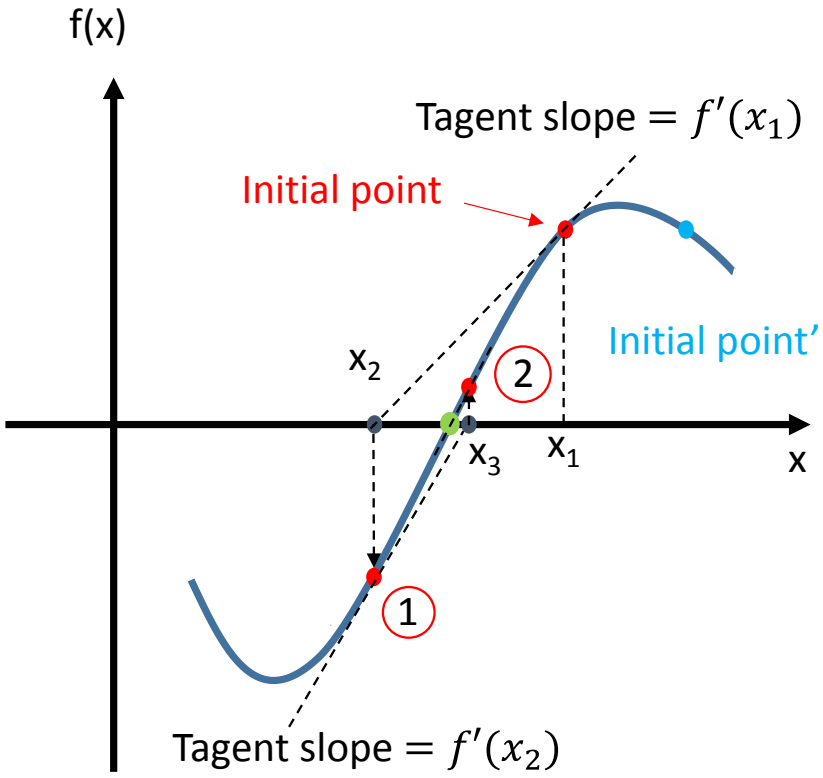

Figure 11. *Process of false position method*

The final option is Taylor approximation method which is used in this thesis. The idea is to use polynomial to approximate the transcendental function $V_g'(t)$, because the polynomial is solvable. Moreover, the Lagrange remainder can be used to control the error of approximation.

Taylor series expansion is used to approximate with a polynomial of the following form:

$$V_g'(t) = V_g'(k) + \sum_{i=1}^{n} \frac{V_g^{(i+1)}(k)}{i!}(t-k)^i + R_n, \tag{19}$$

where k is an arbitrary constant, n is the number or terms, and R_n is the Lagrange remainder which indicates the overall accuracy of the approximation. By taking advantage of the

Lagrange remainder, both the approximation accuracy and the number of terms can be determined. Moreover, the effort of calculation can be saved by smaller term number n corresponding to lower order polynomial series to solve. Since the accuracy is within certain time domain range which has the expression:

$$range = (t-k) = \sqrt[n+1]{\frac{R_n \cdot (n+1)!}{V_g^{(n+1)}(t^*)}}, \tag{20}$$

where it has $t^* \in (t,k)$. Then the range of $V_g^{(n+1)}(t^*)$ is:

$$V_g^{(n+1)}(t^*) = A\sum_{i=1}^{M} \omega_i^{n+1} \cdot \sin(\omega_i^{n+1} t^* + \varphi_i) < A\sum_{i=1}^{M} \omega_i^{n+1}. \tag{21}$$

Due to the characteristic of Taylor expansion, the approximation is accurate at k and less accurate approaching to the edge. Therefore, higher accuracy means a narrower approximating range. After setting R_n and number of terms n, the minimum range of accuracy is determined. Because the range is smaller than the multi-band signal period, multiple times of Taylor expansions are required.

By moving the expansion point multiple times, the approximations will cover the whole period of multiband signal. Fig. 12 shows an example which has the dual-band input signal and the frequency ratio is $f_1 : f_2 = 2:3$. It has the waveform of $V_g(t)$ is:

$$V_g{}'(t) = \cos(2 \cdot 2\pi t) + \cos(3 \cdot 2\pi t). \tag{22}$$

In Fig. 12, the dashed lines are approximation lines and red vertical dash-dot lines shows the expansion point. In total, there are four times of expansions to cover the whole beat period T_{total} which is the reciprocal of beat frequency of the multi-band signal. Since all frequencies

should be integers to the unit of Herz, the beat frequency is the greatest common divisor for all bands frequencies.

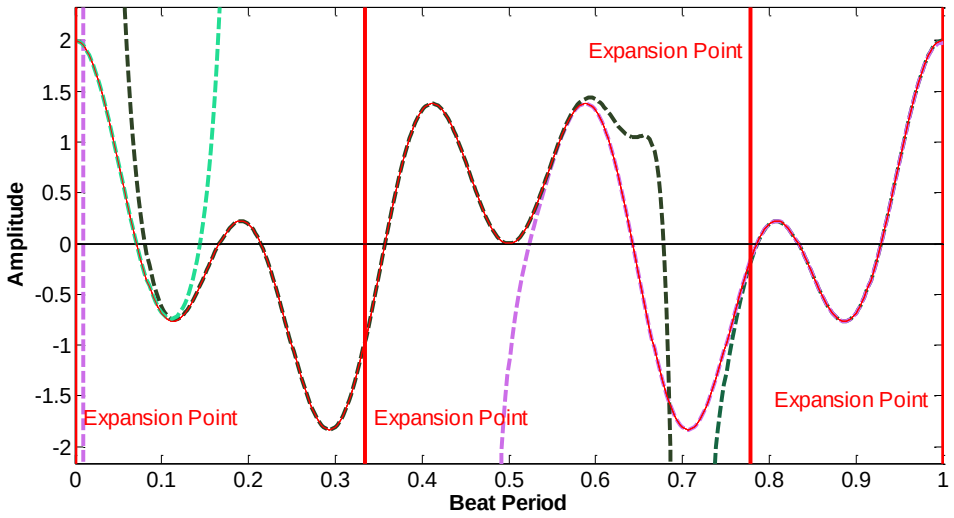

Figure 12. *Multiple Taylor expansion*

Once we have the approximation of $V_g{}'(t)$, it is easy to find the maximum value of the Taylor series polynomial equation within certain range. The global maximum $V_{g,max}$ is achieved by comparing all local maximums and absolute value of minimums. The maximum value is determined by the number of band M, the frequency ratio and the bias point.

After the normalization of $V_g(t)$, it is easy to have the expression of drain current $I_d(t)$ through nonlinear transfer function. An ideal multi-band filter is between drain node and load antenna. The function of ideal filter is picking the amplitudes of fundamental tones from the Fourier transform of drain current. By simply transferring the frequency domain to time domain, the load current has an expression as:

$$I_L(t) = A_{f1}\sin(\omega_1 t) + A_{f2}\sin(\omega_2 t) + \cdots + A_{fM}\sin(\omega_M t), \qquad (23)$$

where the A_f represents the amplitude of fundamental components.

Finally, the drain efficiency is:

$$\eta = \frac{P_{RF}}{P_{DC}} = \frac{I_{L,RMS}V_{L,RMS}}{I_D \cdot V_D} = \frac{I_{L,RMS}^2 R_L}{I_D \cdot I_{L,max} R_L} = \frac{I_{L,RMS}^2}{I_D \cdot I_{L,max}}, \tag{24}$$

where $I_{L,RMS}$ and $I_{L,max}$ are the root-mean-square (RMS) and maximum value of (23), respectively, and I_D is the average value of the drain current given in (6). In order to avoid clipping the drain voltage, the drain should be biased at the maximum value of load voltage which is $I_{L,max} \cdot R_L$. One thing to be noted here, efficiency is expressed with the values of currents because the load impedance are canceled out.

The example which has a frequency ratio $f_1 : f_2 = 2:3$ in class-B mode is shown in shown in Fig. 13. Since the PA operates in class-B mode, the gate voltage $V_g(t)$ is clipped in half from a pure two-tone sine waveform. Accordingly, the drain current $I_d(t)$ has a similar waveform with $V_g(t)$ through the nonlinear transfer function. By choosing the beat frequency as $f_{beat} = 1$, we can plot the drain current in frequency domain $I_d(f)$, which reveals it contains DC component, many harmonics, and IM products. After the ideally filter, only the fundamental components arrives the output port, and the output signal is back to pure two-tone sinewave as $I_L(t)$, from which it is easy to calculate its RMS value $I_{L,RMS}(t)$.

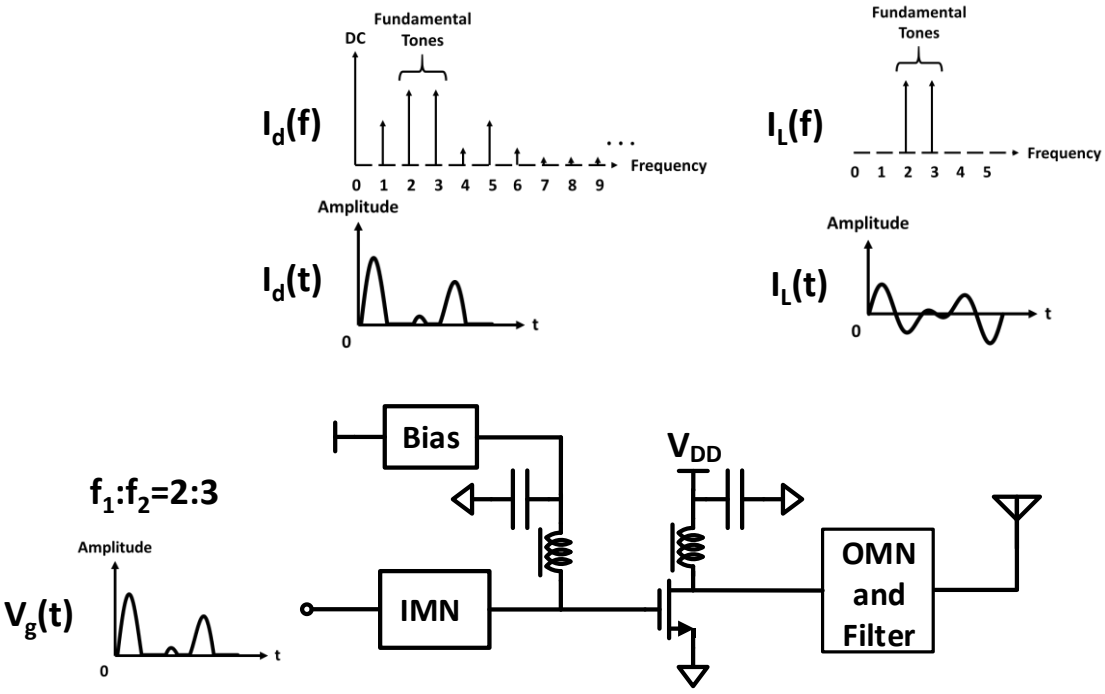

Figure 13. *Concurrent signals in schematic*

The theory of drain efficiency is consistent to class-A, class-B, class-AB, and class-C concurrent linear multi-band PA. The only difference is the bias point of gate voltage V_{gDC}. The drain efficiency results of tri-band concurrent multi-band PAs in different frequency ratios will be shown in Chapter 4.

3.3 Linearity of Multi-Band Power Amplifier

Since the non-linear transistor amplifies the multi-band signals simultaneously, the output signal suffers the nonlinear distortion from each band, which causes more linearity issues in the aspects of gain compression, intermodulation and harmonics.

3.3.1 Gain compression degradation of multi-band PAs

The 1 dB compression point of multi-band is extended into the point power gain drop by 1 dB. As mentioned before, the same amplitude for each band will have worse efficiency and linearity.

The conventional theory assumes the power series after 3rd order has little effect on the amplitude of fundamentals. By expanding (17) to the order of 3 as:

$$I_d(t) = \alpha_1 V_g(t) + \alpha_2 V_g^2(t) + \alpha_1 V_g^3(t), \tag{28}$$

where α_1 , $\alpha_2$and α_3 are the 1st, 2nd and 3rd order coefficients. The values of those coefficients are listed in [17].

As shown in Fig. 14, the blue curve represents gain compression of single-band, and the red curve shows the one band of multi-band gain conversion. To be noted here, the gain compression is between one among M bands for concurrent multi-bands and conventional single-band, however they have the same output power level. For example, with the same normalized nonlinear transferfunction, a comparison of linearity should between concurrent tri-band PA with 3 Watts which each band has 1 watt and a conventional single-band has output power of 1 Watt. The fundamental amplitude of each band of a concurrent multi-band PA is effected by the intermodulations with all the other bands, which has an expression as:

$$A_{fund} = A\alpha_1 + \frac{3}{4}A^3\alpha_3 + \frac{3}{2}A^3\alpha_3(M-1)\,. \tag{29}$$

Similar to conventional single-band, the 1 dB compression point for the concurrent multi-band PA is:

$$A_{1dB} = \sqrt{\frac{4}{3}\left|\frac{\alpha_1}{\alpha_3}\right|} \cdot \sqrt{\frac{0.11}{2M-1}}. \tag{30}$$

The difference is 1 dB amplitude of concurrent multi-band has an extra factor of $\frac{1}{\sqrt{2M-1}}$ which means 1dB compression point of concurrent multi-band PAs will move closer to the origin and become less linear. Moreover, the gain compression issue will be more severe when amplifying more bands of signals simultaneously.

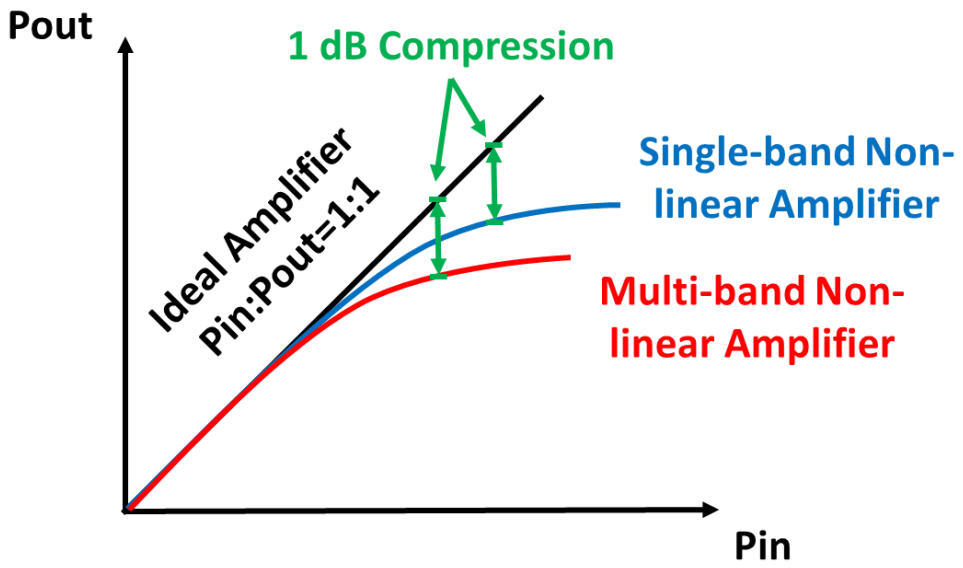

Figure 14. *Gain compression of single-band non-linear amplifier and one band of Multi-band non-linear amplifier*

3.3.2 Intermodulation and harmonics of multi-band PAs

When choosing the frequency ratios for a multi-band PA, there are actually some potential traps. Although people may found some special frequency ratios have higher drain efficiencies, those ratios are highly possible harmonics of other bands or frequency of intermodulation of other bands if the band number M is more than 2.

The reason of higher drain efficiency normally is those harmonics or intermodulation frequencies will behave as current and voltage waveform tuning which reduces the peak-to-average ratio (PAR). For example one band falls on the 3rd harmonic of another band, the sinusoidal voltage and current waveforms is flatten out and DC power consumption is reduced which leads to higher drain efficiency.

However, although it seems more promising with higher drain efficiency, the output power of the bands fall on the harmonics and IMs is not completely applicable. Due to the telecommunication modulation schemes utilize phase modulation, two examples are given here to discuss the output signals containing phase components. The first example is one band falls on the harmonics of another band which will has the input and output signal expressions as:

$$V_g(t) = V_{g1}\cos(\omega_1 t + \varphi_1) + V_{g2}\cos(\omega_2 t + \varphi_2). \tag{31}$$

where φ_1 and φ_2 are phase components to two bands which contains the modulated information. Here the symbol φ can be treated as arbitrary phase modulated scheme which is not pointing at a specific modulation. By setting $\omega_2 = 3\omega_1$ substitute (31) into (28) will have fundamental signal of frequency ω_2 is:

$$I_{L\,\omega_2} = \frac{1}{4}\alpha_3 V_{g1}{}^3 \cos(\omega_2 t + 3\varphi_1) + \alpha_1 V_{g2}\cos(\omega_2 t + \varphi_2)$$
$$+\frac{2}{3}\alpha_3 V_{g1}^2 V_{g2}\cos(\omega_2 t + \varphi_2) + \frac{3}{4}\alpha_3 V_{g2}^3 \cos(\omega_2 t + \varphi_2), \quad (32)$$

The above expression shows the IM3 components of ω_1 and ω_2 will increase the output power. However, the issue is the first element of (32) which is from the third harmonic of ω_1. Since φ represents modulated phase signal, they contains different information when demodulating, if the expressions of φ are not exactly the same. Therefore the first component containing phase $3\varphi_1$ is a noise power to band 2 signal.

The second example is one band is on the third order intermodulation of the other two bands, in order words $\omega_3 = 2\omega_2 - \omega_1$ which shows in Fig. 15. Therefore the noise signal of the fundamental element is:

$$I_{d_{noise}} = \frac{3}{4} V_{g1} V_{g2}^2 \alpha_2 \cos(\omega_3 + 2\varphi_2 - \varphi_1)\,, \quad (33)$$

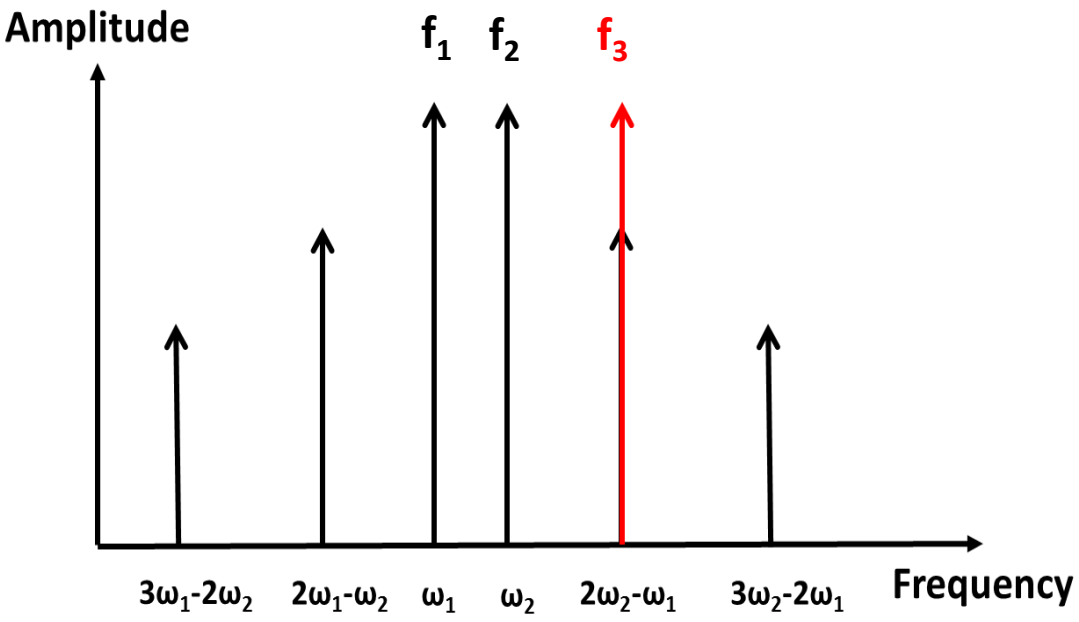

Figure 15. *Noise of third order intermodulation*

Since the errors in (33) have the same frequency with desired signal, which is not able to be filtered out, these frequencies should be avoided when choosing the frequency ratios. In order to remove the ratio that introduce errors, the next task is to find all the harmonics and IMs for an arbitrary frequency ratio. Although it is assumed the system is nonlinear time-invariant (NTI) without memory effect, the Volterra series is needed here to simplify the derivations of input output representation.

In order to find all of the harmonic and IM frequencies, the first thing is to represent the transfer function in the form of Volterra series [18,19] for M-bands and n^{th}-order nonlinearity:

$$y(t) = \sum_{k=1}^{\infty} y_k(t)$$
$$y_k(t) = \frac{1}{2}\sum_{k=1}^{M} \frac{k!\prod_{i=1}^{M} A^{m_i}}{2^{k-1} m_1!\, m_2! \cdots m_M!} H_k e^{j2\pi f_\Sigma t}, \tag{34}$$

where H_k is Fourier transform of the k^{th}-order Volterra kernel, and f_Σ represents all the frequency components and is expressed as:

$$f_\Sigma = \{\underset{m_1}{\pm f_1 \cdots \pm f_1}, \underset{m_2}{\pm f_2 \cdots \pm f_2}, \cdots, \underset{m_M}{\pm f_M \cdots \pm f_M}\}, \tag{35}$$

Where m_i is integer with the range $m_i \in [0, n]$, and

$$\sum_{i=1}^{M} m_i = n\,. \tag{36}$$

For example, when M=4 and n=3, one possible realization of m is {2,0,1,0} which means $f_\Sigma = \pm f_1 \pm f_1 \pm f_3$ resulting the following three locations of nonlinear distortions: $2f_1 + f_3$, $2f_1 +$

f_3, and $= f_3$. All of the harmonics and intermodulation products can be found according to the expression of f_Σ.

For completeness, the amplitude of the nonlinear distortion components can also be extracted from (34) as:

$$A_{NL} = \frac{n!}{2^{n-1} m_1! \, m_2! \ldots m_M!} \frac{1}{A} \prod_{i=1}^{M} (A^{m_i}) \frac{H_n}{H_1}, \tag{37}$$

where H_n/H_1 is able to be simplified by Taylor series coefficients α_n/α_1 [20] because the system is assumed to be the time invariant. Assuming that amplitude of each band is the same, the power ratio between desire signal and distortion is:

$$\frac{P_{NL}}{P_{desire}} = \left(\frac{A_{NL}}{A}\right)^2 = \left(\frac{1}{A^2} \frac{n!}{2^{n-1} m_1! \, m_2! \ldots m_M!} \prod_{i=1}^{M} (A^{m_i}) \frac{\alpha_n}{\alpha_1}\right)^2. \tag{38}$$

CHAPTER 4

SIMULATED EFFICIENCY RESULTS

4.1 Drain Efficiency of 2-D Frequency Ratio Map

In order to display the ideal performance of concurrent multi-band PAs, input signals uses multi-band frequencies with equal amplitudes, because the equal amplitudes for each band will have the worst performance. The initial phases of all bands are set to be zero since the phase differences only make small effects on the total drain efficiency.

The input concurrent tri-band signal (M =3) has the expression:

$$V_g(t) = V_g \sin(\omega_1 t) + V_g \sin(\omega_2 t) + V_g \sin(\omega_3 t)\,. \tag{39}$$

With the same amplitudes and zero initial phase, the only parameter effecting drain efficiency is the frequency ratio. By setting f_1 as a reference as $f_1 = 1$, a 2D plot can be plotted by sweeping frequency ratios f_2/f_1 and f_3/f_1 in order to represent values of drain efficiency. The sweeping step is set at 0.1, and the total range is from 1 to 10.The dual-band efficiency versus frequency ratio can be read from the x-axis.

The drain efficiency is achievable for each frequency ratio by the method of Chapter 3, which the simulated result is shown in Fig. 16 to Fig. 18. In those three figures, each pixel represents the drain efficiency value of the frequency ratio. The darker the pixel is, the higher the efficiency will be.

Meanwhile, once the frequency ratios contain harmonics or IM products, the efficiency will be ignored because harmonic and intermodulation products introduce noise. All the harmonics and IM products are marked as dashed green lines in Fig 12 by the methods of

Chapter 3. The lines start from origin and radiate are the harmonics. In 2-D frequency plot the IM products are the lines parallel to x-axis, y-axis and 45 degree line.

Although the harmonics and IM products are removed from the whole map, drain efficiency still varies from 22% to 29% holding the variation as 7% for class-A concurrent multi-band PA. However, the white color, which is the lowest efficiency, occupies the largest portion. The black color has several dotted lines because of the discrete frequency ratio.

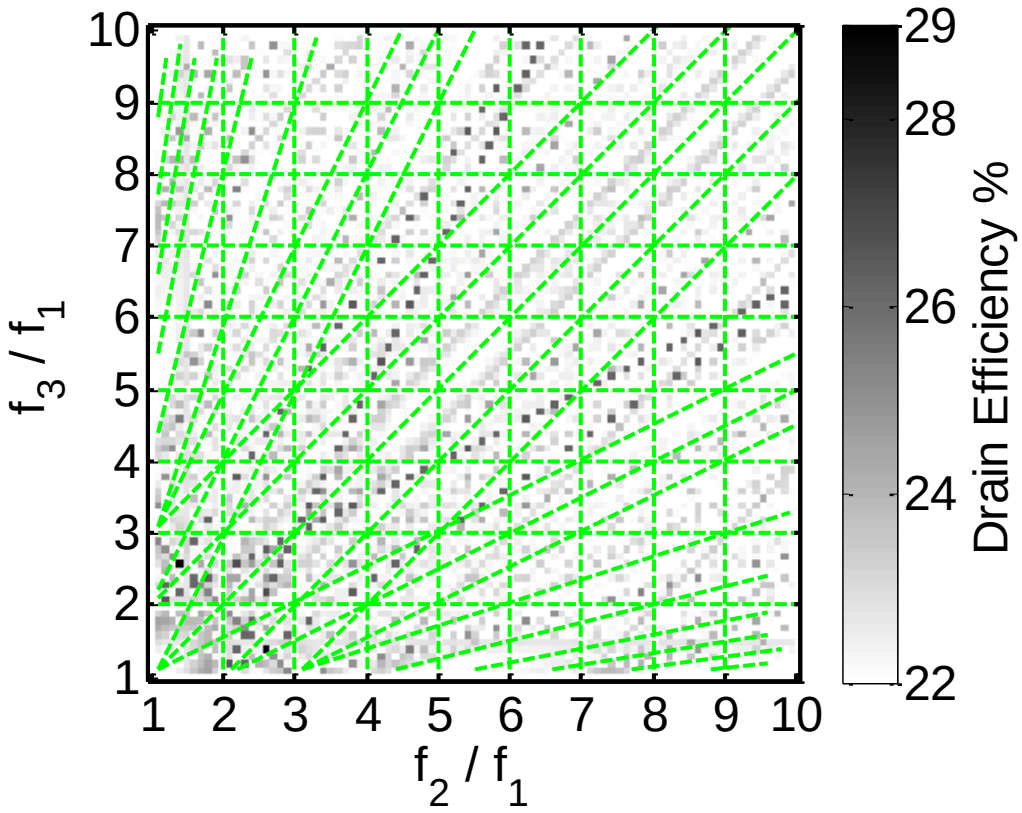

(a)

Figure 16. *Simulated drain efficiency versus 2-D frequency ratio for class-A*

The same method is applied to class-B and the result is shown in Fig. 17. It is apparent that class-B has higher efficiency about from 54% TO 67%, which the variation is 13%.

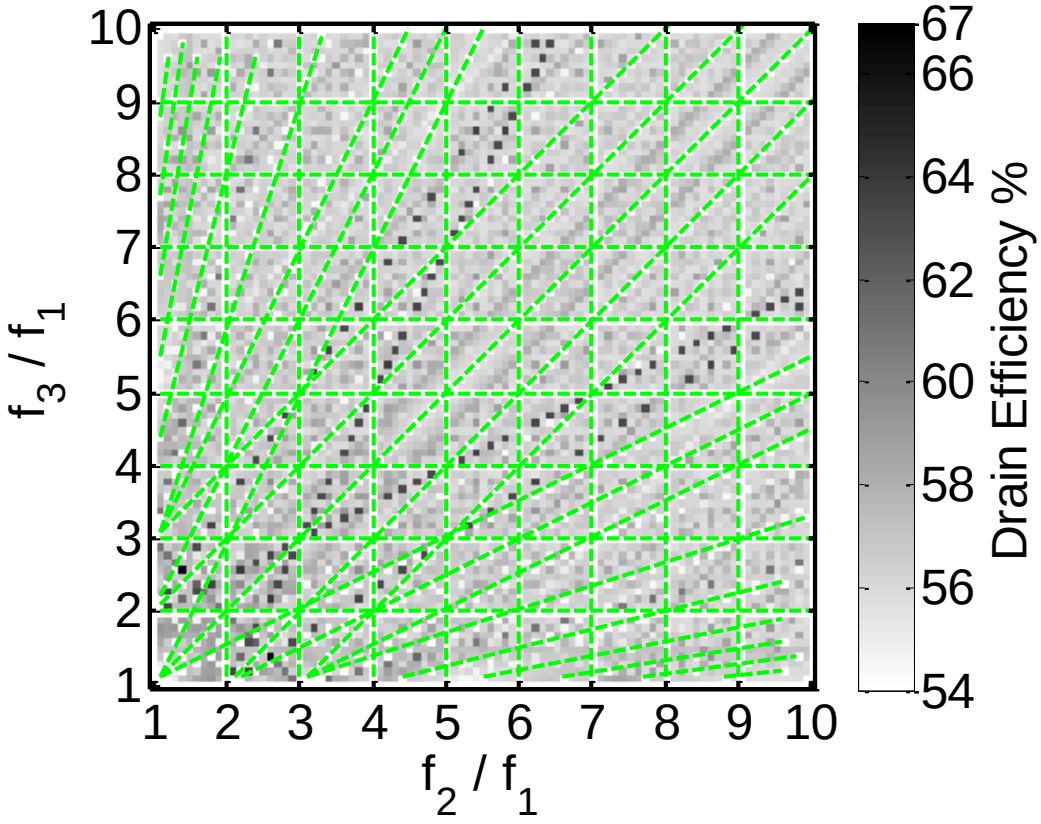

Figure 17. *Simulated drain efficiency versus 2-D frequency ratio for class-B*

Fig. 18 shows the efficiency versus frequency ratio map of class-C. As expected, the tri-band class-C has efficiency from 81% to 91%, which achieves 10% variation. More darker lines are indicating the class-C has larger possibility to have higher efficiency than class-A and B.

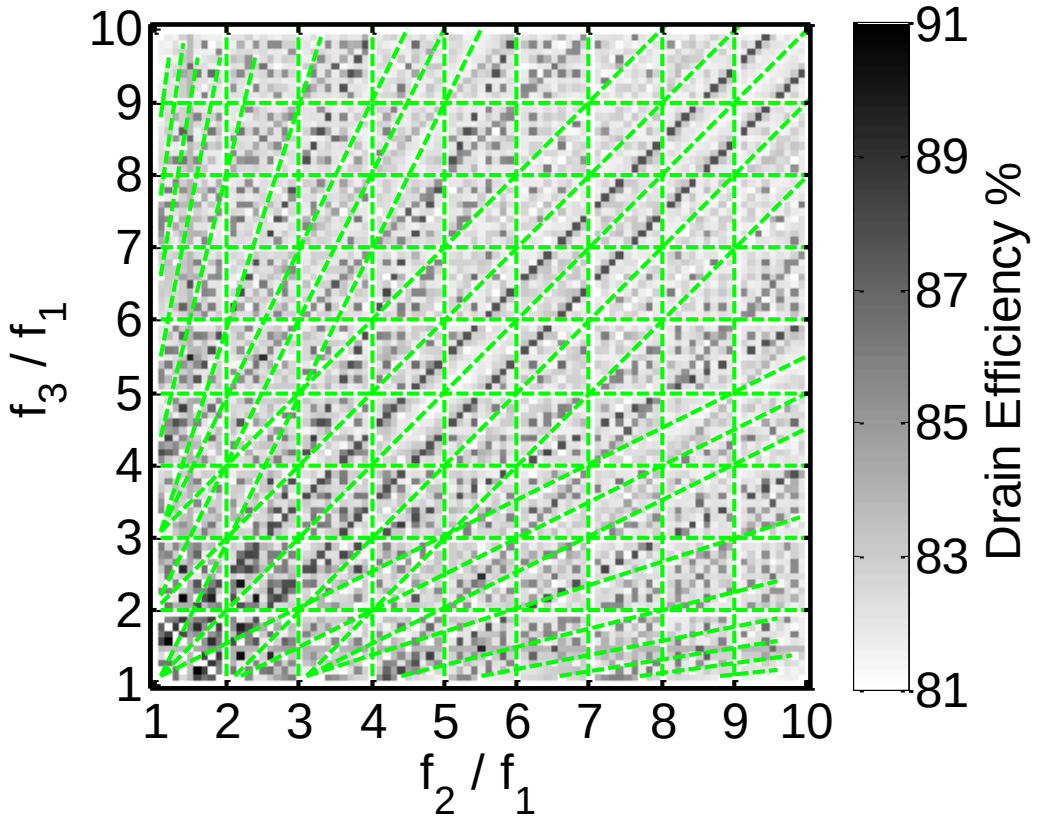

Figure 18. *Simulated drain efficiency versus 2-D frequency ratio for class C*

Here the comparison of drain efficiency between concurrent multi-band and parallel single-band is based on a assumption that the power combiner of parallel single-band architecture is ideal. However, even the lowest insertion loss of the commercial product is 0.2 dB, it means 4.5% of the drain efficiency will drop directly through the power amplifier. However, the bigger issue is the size of multiplexer commercial products are quite large to the perspective of power amplifier which is not applicable for mobile devices. The designs of power combiner based on Wilkinson structure will have smaller size but theoretically 3 dB loss, which leads the drain efficiency drop by half. Then, the power combiners in Wilkinson structure is not applicable for power ampler. Therefore, the drain efficiency performance of parallel single-band is heavily depends on the design of power combiner.

4.2 Drain Efficiency With The Effect of PAR

The variation of drain efficiency over frequency ratios is due to the variation in the peak-to-average ratio (PAR) in the drain current that results from summing different carrier frequencies and can be expressed as: $PAR = I_{dmax}/I_{DC}$. This is illustrated more clearly in Fig. 19 which shows two different drain current waveforms: I_{d1} with $f_2/f_1 = 1.4$ and $f_3/f_1 = 2.6$ and I_{d2} with $f_2/f_1 = 1.8$ and $f_3/f_1 = 3.4$. The drain current, I_{d1}, has a PAR1 = 5.29resulting in $\eta_1 = 62.1\%$. The drain current, I_{d2}, has a PAR2 = 6.16 resulting in $\eta_2 = 54.3\%$, a drop of approximately 8%.

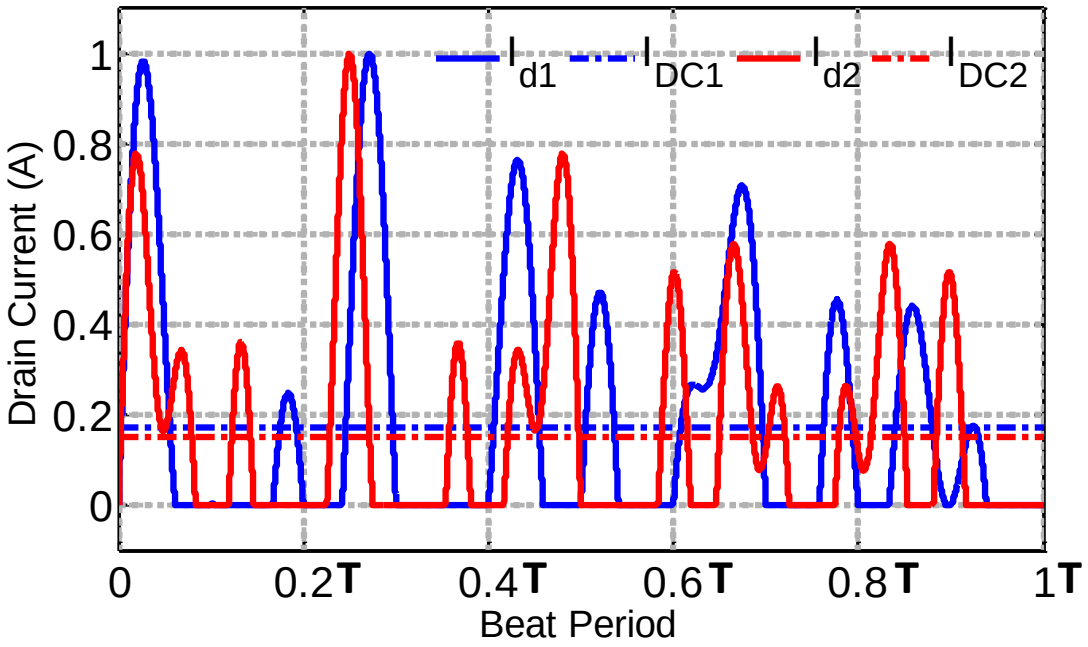

Figure 19. *Class-B drain current and DC current illustrating different PAR. PAR_1=5.29, η_1=62.1%, and PAR_2=6.16, η_2=54.3%.*

It must also be pointed out that the overall efficiency will depend upon the number of supported bands. When the results shown in Fig. 19 are compared to the case when $M = 2$

(dual-band) it is seen that there is a drop in overall efficiency. The efficiency for a concurrent dual-band class-A, class-B, and class-C PA is 30.5%–33.8%, 66.2%–73%, and 84.5%–94.6%, respectively. Notice that the maximum drain efficiency for tri-band class-A is approximately 4% below the minimum efficiency for a dual-band class-A. Finally, the efficiency of the parallel single-band architecture for class-A, class-B, and class-C operation was 50%, 78.3%, and 83%, respectively.

4.3 Possibilities of Drain Efficiency

Fig. 20 shows the probability of achieving a given efficiency for both concurrent multi-band and parallel single-band architectures each with $M = 2$ and $M = 3$.

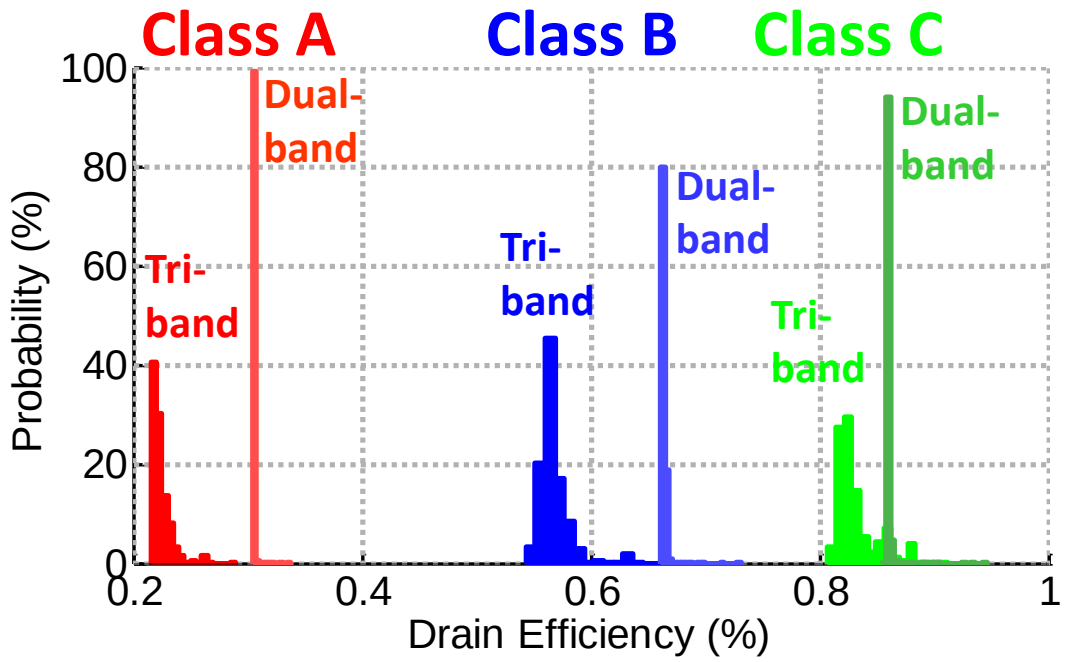

Figure 20. *Probability distribution of drain efficiency for concurrent dual-band and tri-band operation for class-A, class-B and class-C modes of operation*

CHAPTER 5

SUMMARY AND CONCLUSION

In this thesis, the comparison between parallel single-band and concurrent multi-band architectures is established in three aspects, namely area, drain efficiency and linearity. Theoretical least area consumption comparison is presented for both architectures. Quantitative methods of calculating drain efficiency of concurrent multi-band has been developed with more general non-linear transistor model. The linearity issues have been addressed in both gain compression and intermodulation distortion aspects for concurrent multi-band PAs. Simulation results of drain efficiency map for ideal concurrent dual-band and tri-band PAs are shown in the form of 2-D frequency ratios figure. The efficiency distribution has been compared between concurrent dual-band PAs and concurrent tri-band PAs.

Due to all the those analysis, an theoretical concurrent multi-band PA requires much less area, but shows less promising performances on both drain efficiency and linearity than single band in class-A, class-B and class-C. Furthermore, both drain efficiency and linearity are dropping when number of band increasing for concurrent multi-band PAs. According the results of analysis, only class-B and C are applicable options. While the class-A become less viable because the severe low efficiency in multi-band mode. Ideally, parallel single-band PAs have better drain efficiency and linearity. However when implementing parallel single-band PAs, the size of power combiner will be too large for mobile devices. Moreover, the power combiner is also a limit to the drain efficiency. For designers requires higher performance but not size, parallel single-band is a good option. However, it is more promising to design efficiency boost or linearity compensate concurrent multi-band PAs for mobile devices.

REFERENCES

[1] N. Q. Bolton, "Mobile Device RF Front-End TAM Analysis and Forecast," in *CS MANTECH Conference*, 2011.

[2] U.S. DEPARTMENT OF COMMERCE, "United States Frequency Allocations The Radio Spectrum," Aug 2011.

[3] S. A. Bassam, W. Chen, M. Helaoui, and F. M. Ghannouchi, "Transmitter architecture for CA: Carrier aggregation in LTE-advanced systems," in *IEEE Microw. Mag*., vol. 14, no. 5, pp. 78–86, May 2013.

[4] K. Chen, E. J. Naglich, Y. Wu, and D. Peroulis, "Highly linear and highly efficient dual-carrier power amplifier based on low-loss RF carrier combiner," in *IEEE Trans. Microw. Theory and Tech.*, vol. 62, pp. 590-599, Mar. 2014.

[5] Y. Li, Z. Zhang, and N. M. Neihart, "Switchless Matching Networks for Dual-Band Class-E Power Amplifiers," in *IEEE Midwest Symposium on Circuits and Systems*, pp. 555-558, Aug. 2014.

[6] N. Nallam and S. Chatterjee, "Multi-band frequency transformations, matching networks and amplifiers," in *IEEE Trans. Circuits Syst. I, Reg. Papers*, vol. 60, no. 6, pp. 1635–1647, Jun. 2013.

[7] X. Fu, D. Bespalko, and S. Boumaiza, "Novel dual-band matching network for effective design of concurrent dual-band power amplifiers," in *IEEE Trans. Circuits Syst. I, Reg. Papers*, vol. 61, no. 1, pp. 293–301, Jan. 2014.

[8] X. Chen, W. Chen, F. Ghannouchi, Z.Feng, and Y. Liu, "Enhanced Analysis and Design Method of Concurrent Dual-Band Power Amplifiers With Intermodulation Impedance Tuning," in *IEEE Trans. on Microw. Theory and Tech.*, vol. 61, no. 12, pp.4544-4558, Dec. 2013.

[9] D. Pozer, "Microwave Amplifier Design," in *Microwave Engineering*, 4th ed, Hoboken, NJ, US: Wiley, 2011, ch. 12, sec. 5, pp. 596-601.

[10] M. K. Kazimierczuk, "Class AB, B, and C RF Power Amplifiers," in *RF Power Amplifiers*, Chichester, West Sussex, United Kingdom: Wiley, 2008, ch. 3, sec. 3, pp. 82-89.

[11] Genesys Webcasts, Class Lecture "Power Amplifier Design For LTE" Keysight Technologies Inc., SanFransisco, CA, US, Mar. 2010.

[12] M. Chongcheawchamnan, S. Patisang, M. Krairiksh, and I. D. Robertson, "Tri-band Wilkinson power divider using a three-section transmission line transformer," in *IEEE Microw. Wireless Compon. Lett.*, vol. 16, no. 8, pp. 452–454, Aug. 2006.

[13] M. Hayati, S. Malakooti, and A. Abdipour, "A Novel Design of Triple-Band Gysel Power Divider," in *IEEE Trans. Microw. Theory and Tech.*, vol. 61, no. 10, pp. 3558–3567, Aug. 2013.

[14] Q.-X. Chu, F. Lin, Z. Lin, and Z. Gong, "Novel design method of triband power divider," in *IEEE Trans. Microw. Theory and Tech.*, vol. 59, no. 9, pp. 2221–2226, Sep. 2011.

[15] Microlab, "700/850/PCS-AWS Triplexer," BK-37N datasheet, Sep. 2013.

[16] ClearComm Technologies, "Multi-Band Combiner," CCDP-643-1W datasheet.

[17] S. C. Cripps, "Introduction," in *RF Power Amplifiers for Wireless Communications*, 2nd ed. Boston, London, United Kingdom: Artech House, 2006, ch.1, sec. 4, pp. 6-9.

[18] J. W. Graham and L. Ehrmen, "Modeling and Analysis of Quasi-Linear Systems," in *Nonlinear System Modeling and Analysis with Application to Communication Receivers*, Rome, NY: Rome Air Develop. Ctr., Jun. 1973, ch. 1, sec. 7, pp. 27-30.

[19] S. A. Maas, "Volterra-Series and Power-Series Analysis," in *Nonlinear Microwave and RF Circuits*, 2nd ed. Boston, London, United Kingdom: Artech House, 2003, ch. 4, sec. 4, pp. 225-231.

[20] H. Zhang ECEN 655,Class Lecture, Topic "Volterra Series: Introduction & Application," US, 2008.